TECHNICAL RESEARCH REPORT

SYSTEMS RESEARCH CENTER

Supported by the National Science Foundation Engineering Research Center Program (NSFD CD 8803012), Industry and the University

Adaptive Friction Compensation for Bi-Directional Low-Velocity Position Tracking

by N.E. Leonard and P.S. Krishnaprasad

TR 92-91

Adaptive Friction Compensation for Bi-Directional Low-Velocity Position Tracking [1]

Naomi Ehrich Leonard and P. S. Krishnaprasad

Electrical Engineering Department
&
Systems Research Center
University of Maryland
College Park, MD 20742

Abstract

This paper presents a comparative investigation of friction-compensating control strategies designed to improve low-velocity position tracking performance in the presence of velocity reversals for servomechanisms. The methods considered include adaptive control and estimation-based control. Additionally, the various controller designs incorporate different friction models ranging from classical friction and Stribeck friction to the less popular Dahl friction model. This investigation of friction models is motivated by the fact that there is little consensus in the literature on how best to model friction for dynamic friction compensation. The control strategies are compared in an extensive test program involving sinusoidal position trajectory tracking experiments on a direct-drive dc motor. We focus attention on comparative experimental results of friction compensation especially with repeated velocity reversals. The results show that the adaptive and estimation-based controllers outperform more traditional linear controllers. The

[1]This research was supported in part by the National Science Foundation's Engineering Research Centers Program: NSFD CDR 8803012 and by the AFOSR University Research Initiative Program under grant AFOSR-90-0105.

experiments also yield insight into the appropriateness of the different friction models under the tested operating conditions. *In particular, the Dahl model, typically ignored in the literature, proves to be significant for the friction-compensating control problem with repeated zero-velocity crossings.*

1 Introduction

Recent growth in the number and variety of robotics applications has led to a demand for increased precision in robotic manipulation. For example, robots that perform exacting industrial assembly tasks or manipulators employed in delicate surgical procedures must be capable of precisely controlled maneuvering. However, robotic manipulators must contend with *friction* which poses a serious challenge to precise manipulator control. Specifically, failing to compensate for friction can lead to tracking errors when velocity reversals are demanded and oscillations when very small motions are required. To compensate for friction it is best to have some knowledge of the structure of friction, yet there is little overall agreement in the literature on how best to model friction. Further, friction compensation is complicated by the fact that friction parameters vary with temperature and age.

Traditionally, control engineers have used open-loop smoothing techniques, such as dither and pulse-width modulation, to compensate for friction in mechanical systems. However, these techniques have disadvantages, for example, dither can cause mechanical problems such as fatigue by exciting vibrations in manipulators.

As an alternative to these techniques, recent work has brought to the forefront adaptive and estimation-based control techniques for compensation of friction in mechanical systems [1, 2, 3, 4]. Among the compensators proposed in the literature, a variety of friction models are assumed. Much of this work shows experimental evidence that a particular friction model together with a suitable compensation technique improves system

performance. However, since each research team performed different experiments, there is no easy way to compare the relative effectiveness of the different control-technique and friction-model combinations. It should be noted that because there are still uncertainties as to how friction affects dynamic behavior, it is necessary that the true test of control strategies be experimental.

Additionally, much of the recent work in the literature has emphasized friction compensation during uni-directional servomechanism tasks [5]. However, robotic manipulators are often required to perform repetitive tasks, e.g., in welding procedures and in assembly operations, and such bi-directional tasks force the servomechanism to regularly pass through zero velocity where friction behavior is most difficult to control. As a result, there is a need for investigation of friction compensation during velocity reversals.

This paper presents experimental results that exhibit the relative effectiveness of five different friction-compensating controllers. The experiments involve position trajectory tracking with velocity reversals to exercise the problems associated with friction at near-zero velocities and the discontinuous nature of friction at zero velocity. Of the five controllers tested, two are modified versions of adaptive controllers designed in [1] and [3], respectively. Each assumes the classical model of friction. *However, in the present study both adaptive controllers have been upgraded to include more detailed friction elements such as asymmetries and Stribeck friction.*

The third controller tested is a modified version of the estimation-based friction-compensating controller of Walrath [2]. This controller design is based on the Dahl friction model which predicts a first-order dynamic model of friction as a function of displacement with a time constant that is a linear function of velocity. Whereas Walrath was unable to experimentally derive this linear time constant function, the experiments described in this paper successfully verify Dahl's prediction. Additionally, an original stability proof for the estimation-based controller that uses the passivity formalism is discussed in this paper. The verification of the Dahl model and the success of this control strategy in our work is noteworthy because the Dahl model is often ignored in

robotic control problems with high force actuators.

The fourth controller tested is a linear controller with dither. This controller is included as a prototype smoothing controller. The benchmark for the test program is a conventional linear controller with optimized proportional, integral, and derivative (PID) gains and a feedforward acceleration term.

The experimental program, designed for the hardware available in the laboratory, provides a realistic servomechanism control problem. The subject of the program is a direct-drive brush-type dc motor, digitally controlled by means of an IBM AT personal computer (PC). The same series of sinusoidal position trajectory tracking experiments are performed on the motor with each of the five controllers. Tracking performance is measured by root-mean-square (RMS) position error which provides some averaging of external effects. Nonetheless, unmodelled effects such as torque ripple and digital sampling rate are addressed with additional experimentation.

Section 2 of this paper describes a selection of different models of friction found in the literature with a discussion of how each feature of friction influences servomechanism dynamics. Section 3 discusses friction-compensating control strategies and presents the design of the adaptive and estimation-based controllers tested experimentally and the new stability proof of the latter controller. Section 4 provides the details of the experimental program and the experimental results. Conclusions along with some suggestions for future work are given in Section 5.

2 Friction Structure and Dynamics

Using both theory and experimentation, researchers in a number of fields have developed several different models of the structure and dynamics of friction. In selecting a friction model for our dynamic friction-compensating control problem, it is important to consider how the various identified features of friction influence the dynamics of a

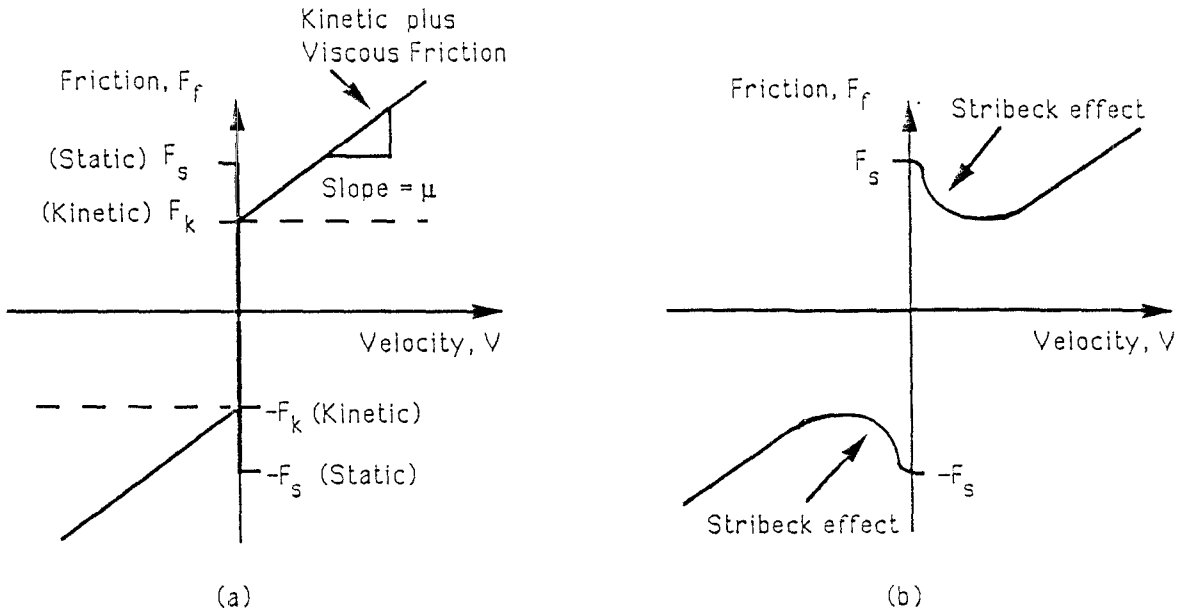

Figure 1: (a) Classical Model of Static, Kinetic and Viscous Friction and (b) Stribeck Friction

servomechanism.

Although rolling friction is a physically different phenomenon from rubbing or sliding friction, the models discussed below attempt to describe the dynamics of a system with rolling *or* sliding friction. Pure rolling friction conditions occur when the contact between two surfaces is a point. However, according to [6], the contact region between two surfaces is typically of larger area than a point because of elastic (and possibly plastic) deformation on one or both of the surfaces. The resulting "rolling" friction in this case involves a combination of sliding and pure rolling friction. In fact, although the sliding velocity is usually small compared to the rolling velocity, sliding friction often provides the major component of the total friction. Consequently, it is appropriate to consider the same models for sliding friction and "rolling" friction.

Classical friction is the earliest and most widely used model of friction. The three components of classical friction: kinetic friction, viscous friction, and static friction, are illustrated on the friction versus velocity graph of Figure 1(a). Although kinetic friction simply provides a constant retarding force to rubbing surfaces, it also introduces a discontinuity at zero velocity. As a result, servomechanisms performing bi-directional tasks

will be subject to the discontinuity during every velocity reversal. The discontinuous behavior of kinetic friction can be classified as a "hard nonlinearity". It is well-known that a closed loop system with a hard nonlinearity can produce a limit cycle, i.e., self-sustained oscillations, that would lead to poor control accuracy.

Viscous friction results from the viscous behavior of a fluid lubricant layer between two rubbing surfaces. As shown in Figure 1(a), viscous friction is represented as a linear function of velocity.

Static friction is the force required to initiate motion from rest. Typically, the magnitude of static friction is greater than the magnitude of kinetic friction which can lead to intermittent motion known as "stick-slip". Stick-slip manifests itself as repeated sequences of sticking between two surfaces with static friction followed by sliding or slipping of the two surfaces with kinetic friction. For the servomechanism control problem, stick-slip can diminish control accuracy. The stick-slip limit cycling can be avoided if damping and stiffness are sufficiently high.

The classical lumped friction model F_f of static friction F_s, kinetic friction F_k, and viscous friction, which depend on the applied tangential force F, velocity V, and coefficient of viscous friction μ, is as follows:

$$F_f = \begin{cases} F_k sgn(V) + \mu V & \text{if } V \neq 0 \\ F_s sgn(F) & \text{if } V = 0 \end{cases} \tag{1}$$

Some experimentalists have noted that in machines with rubbing parts more complicated and numerous than a single body sliding over a second body, the magnitudes of kinetic, viscous, and static friction are not the same in the positive and negative directions [4, 5, 7]. A more general model of friction that accounts for this asymmetry uses different friction coefficients in the positive and negative directions.

Contrary to the predictions derived from the classical friction model, researchers including Courtney-Pratt and Eisner [8] and others have found experimentally that small relative displacements between two bodies in contact do occur when the applied

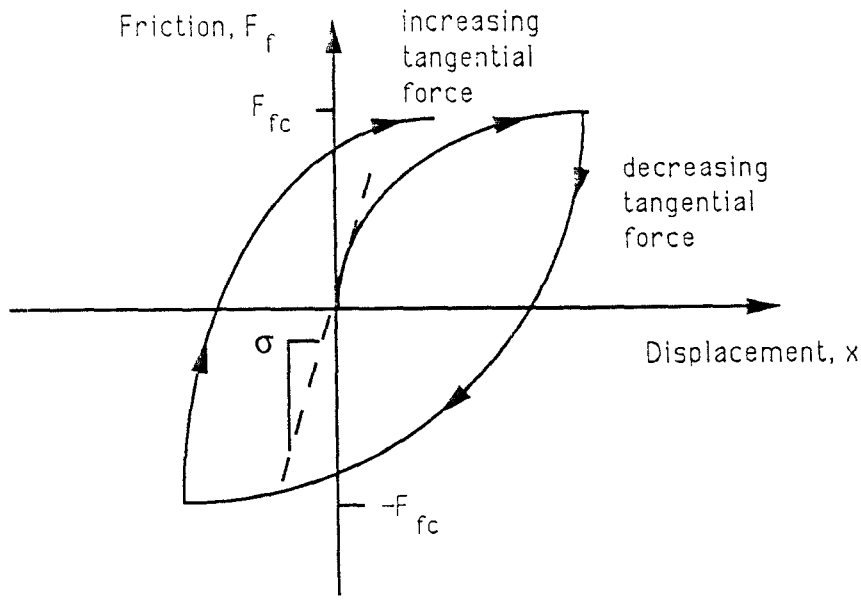

Figure 2: Pre-Sliding Displacement Phenomenon (Dahl Effect)

relative tangential force is *less* than the static friction. Although the magnitude of this pre-sliding displacement is small, with sufficient gain, as in a robot with a fairly long link, small displacements at the rubbing surface can translate into significant displacements elsewhere in the mechanism [5]. Further, the nature of pre-sliding displacements provides insight into the most difficult part of the control problem, the transition between sticking and sliding.

Courtney-Pratt and Eisner interpreted the pre-sliding phenomenon within the framework of the theory of asperity junction adhesion, asperity junctions being the load bearing interfaces between rubbing surfaces. Specifically, as the shear force at the contact surfaces increases, the asperity junctions deform elastically and then plastically. When the applied force finally reaches the static friction level, the asperity junctions break and sliding begins. Because of the plastic deformation, alternate increases and decreases in applied tangential force result in friction hysteresis loops. The pre-sliding displacement phenomenon is illustrated in Figure 2 which shows friction F_f as a function of displacement x based on experimental results.

In [9] the author provided a model of the pre-sliding displacement phenomenon, known as the "Dahl model", that assumes friction F_f is a function of displacement x and time t such that

$$\frac{dF_f(x,t)}{dt} = \frac{\partial F_f(x,t)}{\partial x} \cdot \dot{x} + \frac{\partial F_f(x,t)}{\partial t} , \tag{2}$$

with $\partial F_f/\partial t = 0$, and

$$\frac{\partial F_f(x,t)}{\partial x} = \sigma |1 - \frac{F_f}{F_{f_c}} sgn(\dot{x})|^i . \tag{3}$$

σ and F_{f_c} are as shown in Figure 2, and i is an exponent that Dahl empirically derived to be $i \approx 1.5$.

A friction-compensating adaptive controller based on Dahl's model was designed and successfully used for the stabilization of an airborne pointing and tracking system [2]. Walrath found from experimentation that friction responds continuously to velocity reversals. Using the classical discontinuous static-kinetic friction model, Walrath noted that he could not re-create this smooth behavior. Dahl's model, on the other hand, predicted the expected smooth behavior.

The classical friction model is difficult to use to model friction during velocity reversals because it predicts behavior more characteristic of a system that spends longer periods of time at zero velocity. Specifically, the magnitude of static friction is dependent on the length of time the surfaces are at rest, i.e., the "dwell time". This dependence of static friction on dwell time is, however, useful to explain why under stick-slip conditions the amplitude of the stick-slip limit cycle is observed to decrease with increasing velocity [10].

While the simple static plus kinetic friction model offers an intuitive explanation for the possibility of stick-slip oscillations, it does not offer adequate justification for the existence of these limit cycles in the wide range of conditions under which they have been observed. However, several researchers, e.g., [5] have found a source for this discrepancy in the Stribeck effect, an experimentally derived model of friction variation with velocity as depicted in Figure 1(b). The implications of the Stribeck effect for servomechanism

dynamics include an increased likelihood of stick-slip limit cycling at low velocities. Of the many empirical models derived for friction incorporating the Stribeck effect, the following is the most popular:

$$F_f(V) = F_k sgn(V) + \mu V + (F_s - F_k)e^{-(V/V_{str})^2} sgn(V) \ . \tag{4}$$

where V_{str} is the critical Stribeck velocity.

Frictional lag is one other feature of friction that may also have a significant impact on dynamics. While we do not consider this in the present study, we note the considerable empirical evidence that has recently become available indicating that friction does not respond instantaneously to a change in velocity. The primary work here is due to geophysicists [11] who use stick-slip for earthquake-related predictions. Hess and Soom [12] also found strong evidence of frictional lag, in their experiments on a flat steel button rubbing against a rotating steel disk. Frictional lag makes stick-slip instabilities less likely. Because a decrease in friction occurs *slowly* when velocity is increased, stiff systems will not experience stick-slip [5]. We hope to investigate these aspects in future work.

3 Friction-Compensating Control

If a system with friction is linear and is to be operated only at relatively high velocities without changing directions, i.e., without crossing zero velocity, friction can be modelled as a linear function of velocity. Under these conditions, standard PID design techniques can be applied to the dynamics of the linear system with viscous friction with reliable results. On the other hand, if the system is to be operated at low velocities or with direction reversals, then the standard PID design techniques may be unsuitable and tracking accuracy may prove inadequate. Additionally, to prevent limit cycling due to the static-kinetic friction discontinuity at zero velocity or the Stribeck effect, a PID controller must have sufficiently high "damping" K_d and "stiffness" K_p. However, high

gain control has its own practical disadvantages such as introducing instability in a compliant drive train or saturating an actuator.

One common alternative is the use of a dither signal which averages the dynamics of a system with a discontinuity into smooth dynamics that can be more easily controlled by standard techniques. Dither is a high frequency signal added to the error signal in a feedback loop before it is input to the system. If the frequency is chosen to be higher than the cut-off frequency of the system, the high-frequency behavior is filtered out leaving only the low-frequency "average" response.

Pulse-width modulation is another commonly used and effective smoothing technique that also works on the principle of averaging. However, both dither and pulse-width modulation have inherent disadvantages. For example, analysis and prediction of system characteristics such as stability and robustness are difficult to perform when dither or pulse-width modulation is applied. Additionally, dither can cause mechanical problems in a system such as a robot by exciting higher structural modes.

Friction-compensating adaptive and estimation-based controllers are nonlinear controllers that exploit the known structure of friction. Adaptive control strategies, in particular, are naturally suited to the problem of friction compensation because they generate a time-varying control law that tracks slowly varying system parameters, and they provide system identification when an accurate system model is not available. Three adaptive and estimation-based controllers are investigated in this paper.

For reference, the dynamics of the dc motor used in this paper are described by

$$\ddot{\theta}_p(t) + c_1\dot{\theta}_p(t) = -c_2T_f + c_3u(t)\ , \tag{5}$$

where θ_p, $\dot{\theta}_p$, $\ddot{\theta}_p$ are plant angular position, velocity, and acceleration, T_f is the frictional torque and may depend on θ_p, $\dot{\theta}_p$, etc., u is the control input, and c_1, c_2, c_3 are constants (c_1 includes viscous friction).

The first of the adaptive and estimation-based controllers is an adaptive controller

(referred to as AEC I) based on the Model Reference Adaptive Control (MRAC) approach proposed by [1] in their work on control of a satellite-tracking telescope. However, while Gilbart and Winston considered velocity trajectory tracking in their design, the controller in the present paper was required to handle position trajectory tracking. As a result, AEC I is a modified version of the Gilbart and Winston design, incorporating filters to reduce the order of the system.

Additionally, Gilbart and Winston assumed the classical, symmetrical kinetic plus viscous friction model in the dynamic system equations. To accommodate the observed asymmetrical nature of friction in the motor [7], kinetic friction is modelled in AEC I as follows:

$$T_f = \alpha_1 \left(\frac{sgn(\dot{\theta}_p) + 1}{2} \right) + \alpha_2 \left(\frac{sgn(\dot{\theta}_p) - 1}{2} \right) , \tag{6}$$

where α_1 and α_2 represent the magnitude of kinetic friction in the positive and negative directions, respectively.

While Gilbart and Winston used only proportional feedback control in addition to the adaptive control, our controller uses a control input based on the computed torque method with integration in addition to the adaptive control. Figure 3 shows the block diagram for AEC I. A stability analysis of this controller which follows [1] and employs Lyapunov's direct method yields the result that $(e, \dot{e}) = (0, 0)$ is an asymptotically stable equilibrium point where $\dot{e} = \dot{\theta}_m - \dot{\theta}_p$, $e = \theta_m - \theta_p$ and $\dot{\theta}_m$ and θ_m are the ideal model velocity and position, respectively. Details are to be found in [13].

The second controller (referred to as AEC II) is based on the method developed by [3] in his design of an adaptive robotic manipulator controller. As in the work of Gilbart and Winston, Craig used an MRAC approach and assumed the classical, symmetrical model of kinetic plus viscous friction. Four different versions of the AEC II controller are developed, each with a different model of friction. For reference, we solve equation (5) for input u and rewrite as

$$u = (1/c_3)\ddot{\theta}_p + (c_1/c_3)\dot{\theta}_p + (c_2/c_3)T_f = (1/c_3)\ddot{\theta}_p + Q \ . \tag{7}$$

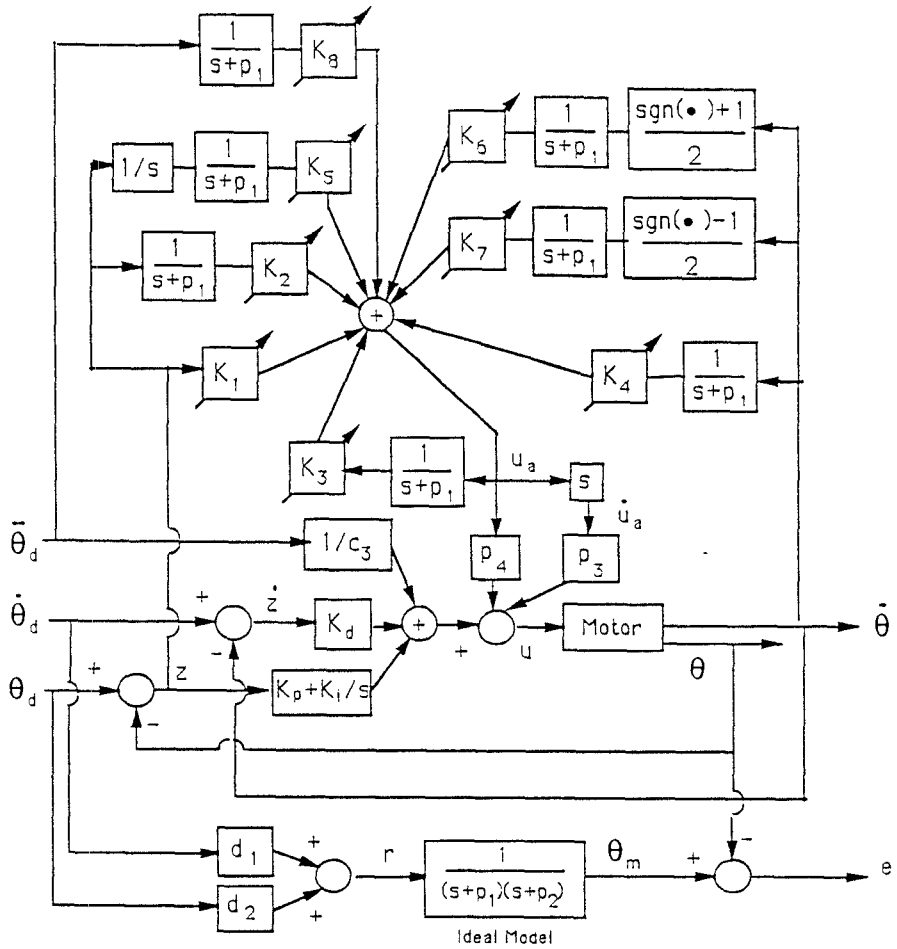

Figure 3: AEC I

Friction model (a) is the simple kinetic plus viscous friction model used by Craig in his design such that

$$Q^{(a)} = p_1\dot{\theta}_p + p_2 sgn(\dot{\theta}_p) \ , \tag{8}$$

where p_1 and p_2 are the unknown viscous and kinetic friction parameters, respectively. Model (b) assumes the asymmetric kinetic plus viscous friction model represented by

$$\begin{aligned} Q^{(b)} \ = \ & p_1\dot{\theta}_p\tfrac{1+sgn(\dot{\theta}_p)}{2} + p_2\dot{\theta}_p\tfrac{1-sgn(\dot{\theta}_p)}{2} \\ & + p_3\tfrac{sgn(\dot{\theta}_p)+1}{2} + p_4\tfrac{sgn(\dot{\theta}_p)-1}{2} \ , \end{aligned} \tag{9}$$

where p_1 and p_2 are the unknown viscous friction parameters in the positive and negative directions, respectively and p_3 and p_4 are the unknown kinetic friction parameters in the positive and negative directions, respectively.

Model (c) includes a linear model of Stribeck friction in addition to kinetic plus viscous friction. Stribeck friction can be modelled according to (4) for $V = \dot{\theta}_p$ and $V_{str} =$

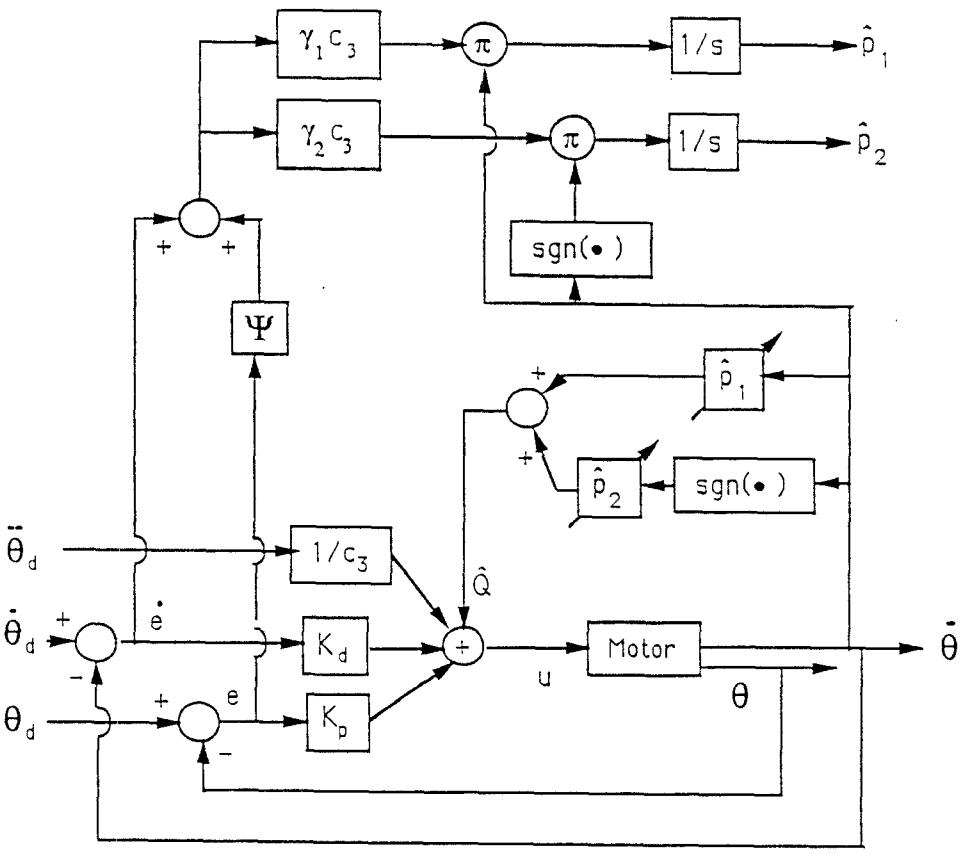

Figure 4: AEC II

$\dot{\theta}_{str}$. However, AEC II requires dynamics that are linear in the unknown parameters. To derive a linear-in-parameters model, the exponential in (4) is replaced by its Taylor series approximation which yields

$$Q^{(c)} = p_1\dot{\theta}_p + p_2 sgn(\dot{\theta}_p) + p_3\dot{\theta}_p{}^2 sgn(\dot{\theta}_p)\ . \tag{10}$$

For comparative purposes, Model (d) includes kinetic plus viscous plus Stribeck friction terms according to the linearized model of [14] such that

$$Q^{(d)} = p_1\dot{\theta}_p + p_2 sgn(\dot{\theta}_p) + p_3|\dot{\theta}_p|^{1/2} sgn(\dot{\theta}_p)\ . \tag{11}$$

The block diagram for AEC II is shown in Figure 4. A stability analysis that follows [3] and uses the Kalman-Yakubovich-Popov Lemma and Lyapunov's direct method shows that $(e, \dot{e}) = (0, 0)$ where $\dot{e} = \dot{\theta}_d - \dot{\theta}_p$ and $e = \theta_d - \theta_p$ (see [13]).

The third controller, AEC III, is an estimation-based controller that follows the work of [2] described in the previous section. From experimental results, Walrath postulated the following first-order model of the bearing friction T_f:

$$\tau \frac{dT_f}{dt} + T_f = T_c sgn(\dot{\theta}_p) \tag{12}$$

where T_c is the rolling bearing friction (i.e. kinetic friction) and τ is a time constant. Clearly (12) is a rewriting of the Dahl friction model of (3) with $i = 1$ and replacing F_f with T_f, F_{f_c} with T_c and x with θ_p where

$$\tau = \frac{T_c}{\sigma |\dot{\theta}_p|} \, . \tag{13}$$

Walrath incorporated the friction model (12) into his controller by using it to predict friction torque. He added the friction torque term to a proportional feedback control input to cancel the friction effect during tracking. The value of τ was also updated by the controller since τ varies with operating conditions (in particular, $\dot{\theta}_p$) as indicated by (13). Since the value of σ from (13) is unknown, Walrath performed a special series of experiments to empirically determine how τ varies with operating conditions. He found τ to be a linear function of the inverse of the RMS system acceleration $\ddot{\theta}_{rms}$. This is *inconsistent* with Dahl's model which predicts that τ is inversely proportional to velocity (13).

On the other hand, we found a *consistent* relationship for τ for the electric motor of the present study. Experiments similar to Walrath's were performed on the motor to determine $\tau = 1/\omega$ as a function of operating conditions. Figure 5(a) shows the results of one series of these experiments. In this series, approximately 56 sinusoidal position trajectory tracking experiments were run, each 320 seconds long. For each of these 56 experiments, the frequency and amplitude of the demanded sinusoidal trajectory were $f = 0.25$ Hz and $A = 0.25$ rad, respectively. Tracking was performed with a controller based on the computed torque method with integration plus a friction cancellation term based on (12). However, we fixed the value of τ for a single experiment and incremented its value only between experiments. Thus, by measuring performance (RMS

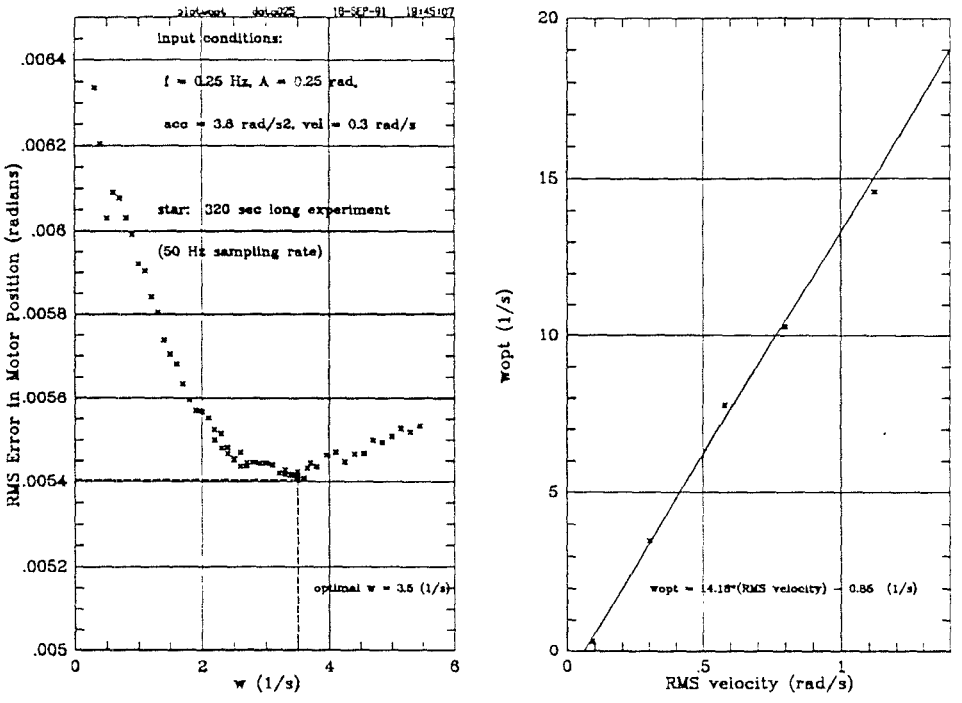

Figure 5: (a) Experimental Results Used to Determine Optimal ω ($f = 0.25$ Hz) and (b) Optimal Values of ω as Function of Operating Conditions

error in motor position) for each experiment, we were able to find the optimal value of τ for the given operating conditions, i.e., the value of τ used in the experiment which produced the lowest RMS position error. For this series of experiments, the "operating conditions" were the measured RMS acceleration of 3.8 rad/s^2 and RMS velocity of 0.3 rad/s common to each experiment in the series.

In Figure 5(a) RMS error in motor position is plotted as a function of $\omega = 1/\tau$. Since a single value of τ is associated with each experiment in the series, each point on the plot represents a single 320-second-long experiment. The optimal value of $\omega = 3.5\ \ s^{-1}$ (ω_{opt}) for the operating conditions associated with this series is read off the plot at the point of lowest RMS position error.

The results of the above series of experiments as well as the results of four other similar series of experiments run at different operating conditions (induced by different

demanded sinusoidal trajectory frequencies) are shown in Figure 5(b). Specifically, Figure 5(b) plots ω_{opt} ($1/\tau$ optimal) as a function of the operating condition, RMS velocity. Each point on this plot corresponds to a single series of experiments. For example, the point at 3.5 s^{-1} (ω_{opt}) versus 0.3 rad/s (RMS velocity) corresponds to the result of the series shown in Figure 5(a). Figure 5(b) shows ω_{opt} to be a linear function of RMS velocity, i.e., the optimal τ is approximately inversely proportional to $|\dot{\theta}_p|$ which is consistent with Dahl's model (13).

AEC III uses the computed torque method with integration plus the predicted friction torque term updated according to (12). The constant τ is adjusted on-line according to the linear function of Figure 5(b). Note that in Walrath's controller, only proportional feedback control was used in conjunction with friction compensation. Figure 6 shows a block diagram of AEC III.

Since Walrath did not provide a stability analysis for his controller, an original stability analysis has been developed based on the passivity formalism. The definitions and theorems of the passivity formalism used below are taken from [15, 16].

Definition: A system of the form

$$\begin{aligned} \dot{x} &= f(x) + G(x)u \\ y &= h(x) + J(x)u \end{aligned} \tag{14}$$

with supply rate (an abstraction of input power associated with the concept of stored energy in a physical system)

$$w(u, y) = y^T Q y + 2y^T S u + u^T R u \tag{15}$$

is dissipative if

$$\int_{t_0}^{t_1} w(t)dt \geq 0 \tag{16}$$

along trajectories of the system (14), for all locally square integrable $u(\cdot)$, all $t_1 \geq t_0$, and $x(t_0) = 0$. If

$$w(u, y) = u^T y - \epsilon y^T y \tag{17}$$

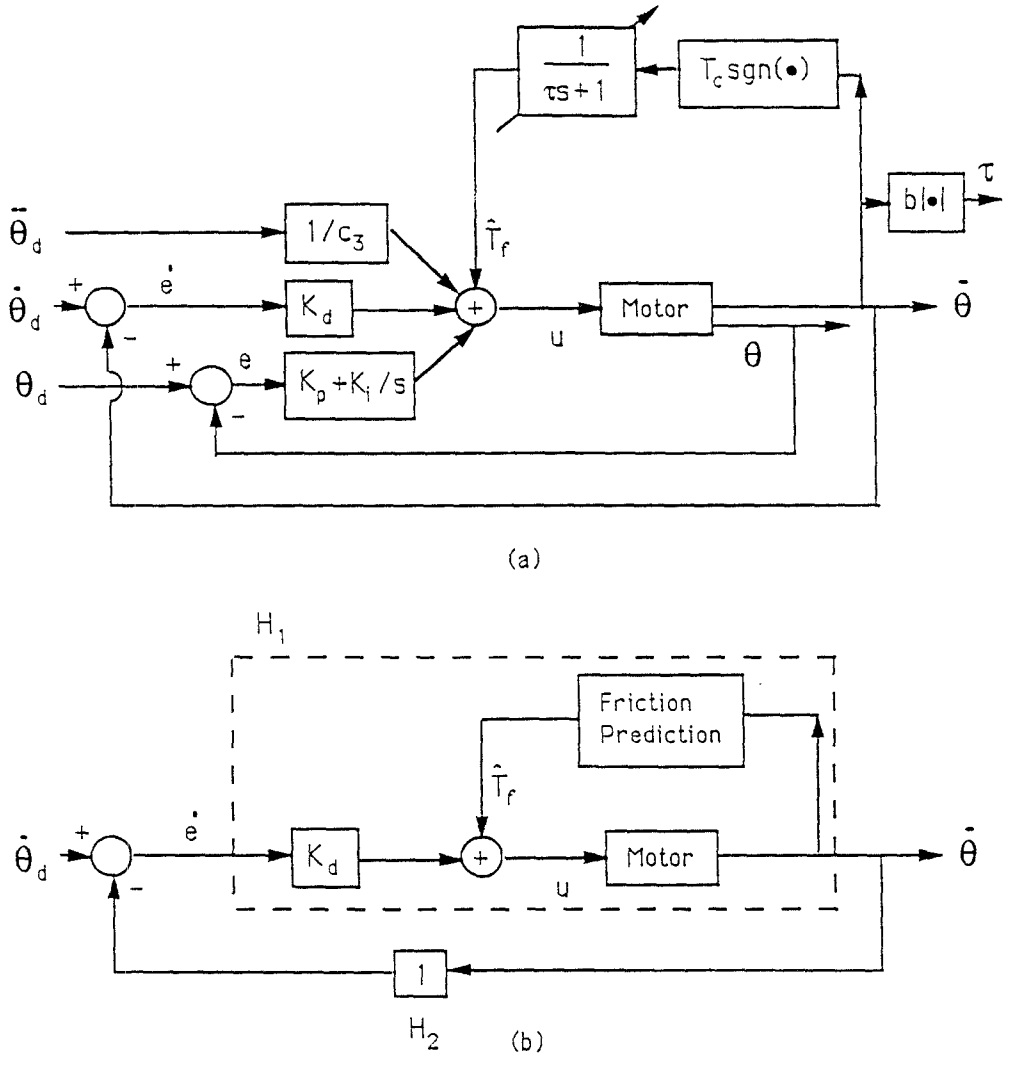

Figure 6: (a) AEC III and (b) AEC III Model for Stability Proof

for $\epsilon > 0$ then the system is Y-strongly passive (YSP).

Consider AEC III with friction prediction and derivative feedback only as shown in Figure 6(b). Let the forward part of the loop including the motor, friction prediction and derivative gain K_d be represented by H_1. The feedback part of the loop is represented by H_2 which implies that $H_2 = 1$. Then it follows from [16], that if both H_1 and H_2 are Y-strongly passive (YSP), the feedback system is asymptotically stable. The fact that $H_2 = 1$ is SPR implies that H_2 is YSP. It remains to prove that H_1 is YSP.

System H_1 can be described by the following equations:

$$\ddot{\theta}_p + c_1\dot{\theta}_p = -c_2 T_f + c_2\hat{T}_f + c_3 K_d\dot{e}\ , \tag{18}$$

$$\dot{T}_f = -b|\dot{\theta}_p|T_f + bT_c\dot{\theta}_p\ , \tag{19}$$

$$\dot{\hat{T}}_f = -\hat{b}|\dot{\theta}_p|\hat{T}_f + \hat{b}T_c\dot{\theta}_p \ . \tag{20}$$

where the $\hat{}$ indicates a predicted value and we have assumed $\omega = b|\dot{\theta}_p|$ and $\hat{\omega} = \hat{b}|\dot{\theta}_p|$.

Define the state $(x_1, x_2, x_3, x_4) = (\theta_p, \dot{\theta}_p, T_f, \hat{T}_f)$ and let $u = \dot{e}$. Then system H_1 can be presented in state-space form as

$$\begin{bmatrix} \dot{x}_1 \\ \dot{x}_2 \\ \dot{x}_3 \\ \dot{x}_4 \end{bmatrix} = \begin{bmatrix} x_2 \\ -c_1x_2 - c_2x_3 + c_2x_4 \\ -b|x_2|x_3 + bT_cx_2 \\ -\hat{b}|x_2|x_4 + \hat{b}T_cx_2 \end{bmatrix} + \begin{bmatrix} 0 \\ c_3K_d \\ 0 \\ 0 \end{bmatrix} u \ , \tag{21}$$

$$y = x_2 \ . \tag{22}$$

Now define $\phi : \mathcal{R}^4 \mapsto \mathcal{R}$ as

$$\begin{aligned} \phi(x) \ = \ & \tfrac{c_2}{c_3KK_d}[\tfrac{K}{2c_2}{x_2}^2 + x_3(x_1 - \gamma_1/b) - \tfrac{1}{2}T_cb(x_1 - \gamma_1/b)^2 + \textstyle\int bx_1x_3|x_2| \\ & + x_4(x_1 - \gamma_2/\hat{b}) - \tfrac{1}{2}T_c\hat{b}(x_1 - \gamma_2/\hat{b})^2 + \textstyle\int \hat{b}x_1x_4|x_2|] \end{aligned} \tag{23}$$

where K, γ_1, and γ_2 are constants to be defined later. Differentiating (23) with respect to time yields the supply rate

$$\dot{\phi}(x) = uy - \epsilon y^2 + \frac{c_2}{c_3KK_d}[x_2x_3 - Kx_2x_3 + \gamma_1|x_2|x_3 + x_2x_4 + Kx_2x_4 + \gamma_2|x_2|x_4] \tag{24}$$

where $\epsilon = c_1/c_3K_d > 0$. First consider the case when $x_2 = \dot{\theta}_p \geq 0$. Then (24) becomes

$$\dot{\phi}(x) = uy - \epsilon y^2 + \frac{c_2}{c_3KK_d}[(1 - K + \gamma_1)|x_2|x_3 + (1 + K + \gamma_2)|x_2|x_4] \ . \tag{25}$$

So choose $\gamma_1 > -1$ and $\gamma_2 < -1$ such that $\gamma_1 + \gamma_2 = -2$, then $K = 1 + \gamma_1 = -1 - \gamma_2 > 0$ and

$$\dot{\phi}(x) = uy - \epsilon y^2 \ . \tag{26}$$

If on the other hand $x_2 = \dot{\theta}_p \leq 0$, then the parameters K, γ_1, and γ_2 can similarly be chosen so that (26) holds.

According to [15] to show that H_1 is dissipative with respect to the supply rate given by (26), $\phi(0) = 0$ and $\phi(x) \geq 0 \ \forall x$ must hold. These do not hold for the function $\phi(\cdot)$

as defined by (23). However, for $x_2 = \dot{\theta}_p \geq 0$ (or $x_2 = \dot{\theta}_p \leq 0$), $x_1 x_3 = T_f \theta_p \geq 0$ and $x_2 x_4 = \hat{T}_f \theta_p \geq 0$. Additionally, x_1 and x_3 are both bounded since $0 \leq x_1 = \theta_p \leq 2\pi$ and $-T_c \leq x_3 = T_f \leq T_c$. Therefore $\phi(\cdot)$ from (23) is bounded below. Define C as the greatest lower bound of $\phi(x)$. Then there exists some $x_0 \in \mathcal{R}^4$ such that $\phi(x_0) = C$. Next define $\tilde{\phi} : \mathcal{R}^4 \mapsto \mathcal{R}$ such that

$$\tilde{\phi}(y) = \phi(y + x_0) - C \; . \tag{27}$$

Then $\tilde{\phi}(0) = 0$ and $\tilde{\phi}(y) \geq 0 \; \forall y$ and $\dot{\tilde{\phi}}(y) = \dot{\phi}(y)$ given by (26). Thus, H_1 is YSP and the feedback system of Figure 6(b) is input-output stable. This implies that $\dot{\theta}_p$ will follow $\dot{\theta}_d$.

4 Experimental Program and Results

The experimental system consisted of a direct-drive, brush-type dc motor, angular position and velocity sensors, a power amplifier, an IBM AT PC, and supporting hardware and software for communication and control. The IBM PC was used to control the operation of the motor. A 50 Hz sampling rate was used throughout the experimental program.

Angular position of the motor was measured by a 12 bit absolute optical shaft encoder. The position data was transmitted to the PC with a measurement resolution of 0.00154 radians (0.088 degrees). A tachometer measured the angular velocity of the motor with a resolution of 0.012 rad/s.

The motor system was modelled according to (5) where u is the input voltage to the motor. For system simulations, friction was modelled as symmetric kinetic plus viscous friction. The friction parameters, assumed to be constant, were measured in previous work by [7]. The motor model was successfully verified by comparing results of voltage pulse experiments on the motor to results of identical simulated experiments on the motor model.

The motor model along with a simulation of a PID controller was then used to design an optimized benchmark PID controller for position tracking. (The controller is actually based on the computed torque method with integration but is equivalent to PID control plus a feedforward acceleration term. *It is referred to as PID control for convenience.*) The PID controller gains were selected to optimize the motor response to a 0.25 radian step demand in angular position. CONSOLE, a numerical optimization tool described in [17], was used to perform the optimization. Two functional objectives were specified, one to minimize the overshoot of the step response and one to maximize the rise time of the step response. The effectiveness of the optimized gains was verified by a 0.25 radian step experiment on the motor.

The experimental program on the electric motor consisted of comparative position trajectory tracking tests using five different controllers: AEC I, II, III, a controller with dither and the optimized benchmark PID controller. The controller with dither was implemented identically to the PID controller except that a dither signal was added to the control input. The frequency of the dither signal was 25 Hz which is the maximum acceptable given the 50 Hz sampling rate. The amplitude of the dither signal was more than twice the magnitude of the static friction.

In each experiment the motor was required to track a sinusoidal position trajectory such that:

$$\theta_d = Asin(2\pi ft) \tag{28}$$

where A is the amplitude and f the frequency of the demanded trajectory. This required sinusoidal motion provided a useful means for investigating friction compensation since the motor was forced to repeatedly pass through zero velocity where friction behavior is most difficult to control. The sinusoidal motion also provided a reasonably realistic scenario since manipulators are often required to perform repetitive tasks that demand sinusoidal joint motions.

The sinusoidal trajectories tracked in the experimental program ranged in frequency

Type of Controller	Trajectory Frequency f (Hz)	RMS Position Error (rad)	Time Elapsed Before Error Calculated (s)	% Error Reduction from PID
PID	1.0	0.0106	0	-
Dither	1.0	-	-	-
AEC I	1.0	0.0048	400	55
AEC II	1.0	0.0079	12	25
AC III	1.0	0.0054	12	49
PID	0.5	0.0069	0	-
Dither	0.5	0.0066	0	4
AEC I	0.5	0.0033	400	52
AEC II	0.5	0.0041	12	41
AEC III	0.5	0.0028	12	59
PID	0.25	0.0063	0	-
Dither	0.25	0.0055	0	13
AEC I	0.25	0.0043	400	32
AEC II	0.25	0.0037	12	41
AEC III	0.25	0.0036	12	43
PID	0.1	0.0060	0	-
Dither	0.1	0.0045	0	25
AEC I	0.1	-	-	-
AEC II	0.1	0.0044	12	27
AEC III	0.1	0.0040	12	33

Table 1: Results of Sinusoidal Tracking Experiments

f from 0.1 Hz to 1.0 Hz. The lower limit of this range was selected to minimize motor velocity and to avoid large errors due to velocity measurement resolution. The upper limit of this range was selected to maximize motor velocity without generating gross errors due to the limitations of the 50 Hz sampling rate. A 0.25 radian amplitude A was used for all sinusoidal trajectory tracking experiments.

The RMS position error for each of the controllers and each experiment is listed in Table 1. Each RMS position error is calculated based on 16 seconds (800 samples) of data. As indicated in Table 1, the controller with dither does not significantly improve the tracking performance as compared to the benchmark PID controller. This is due to the fact that the dither frequency is limited to 25 Hz. AEC I, II, and III, on the other

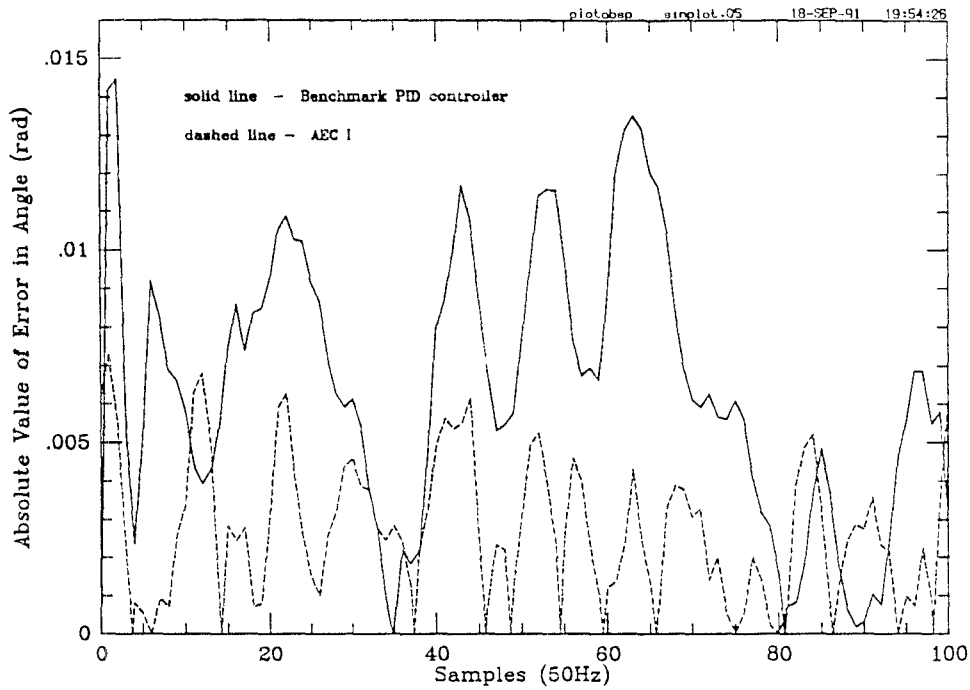

Figure 7: Position Error for AEC I Compared to Benchmark PID Controller

hand, all effectively improved tracking performance for the range of sinusoidal trajectory frequencies tested. The lower values of percent reduction in RMS error for the 0.1 Hz experiment are most likely due to the limited resolution of the position measurements.

Figures 7, 8, and 9 show the absolute value of PID controller position error compared to the position error from AEC I, II, and III, respectively. In each case the PID controller result is shown as a solid line and the nonlinear controller result is shown as a dashed line. Note that the two seconds (100 samples) shown correspond to the first two seconds of the experimental results beginning at the time listed in the fourth column of Table 1.

A comparison of these plots and the performance results of Table 1 suggests that AEC II is not as effective at friction compensation as AEC III. This can be explained by noting that there are a couple of relatively large error peaks in Figure 8 for AEC II. These occur because AEC II overcompensates when friction changes instantaneously. The large error peaks seen in Figure 8 correspond in time to the instantaneous friction

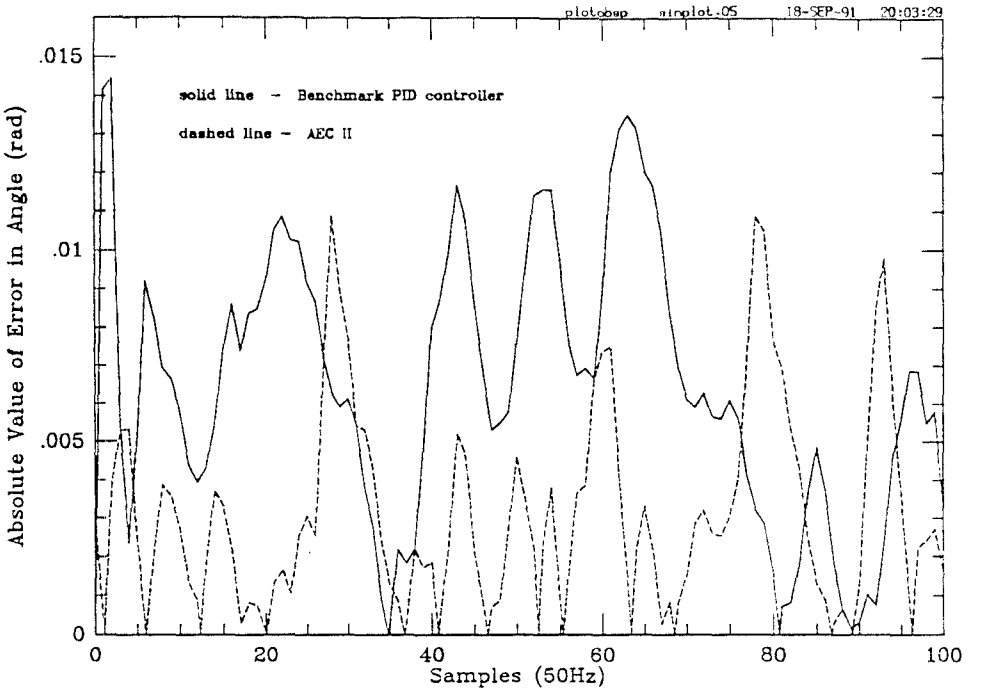

Figure 8: Position Error for AEC II Compared to Benchmark PID Controller

changes. This overcompensation and corresponding large error suggests that the classical friction model does not capture friction during transient velocity reversals as well as the Dahl model.

The numbers listed in Table 1 are averages of results from experiments made over a period of a few days. However, over the course of about six months during which these experiments were performed, there was a great deal of repeatability in the percent reduction in RMS position error achieved by the two adaptive controllers. The experiments were run during different seasons and during different stages of motor "warm-up" such that friction parameters may have varied from experiment to experiment due to temperature differences. Additionally, over the six month period the friction parameters may have changed due to system aging. The fact that the adaptive controllers were consistently effective under these varying conditions provides evidence for the effectiveness of the adaptability of these controllers.

The results for AEC II provided in Table 1 correspond to experiments performed

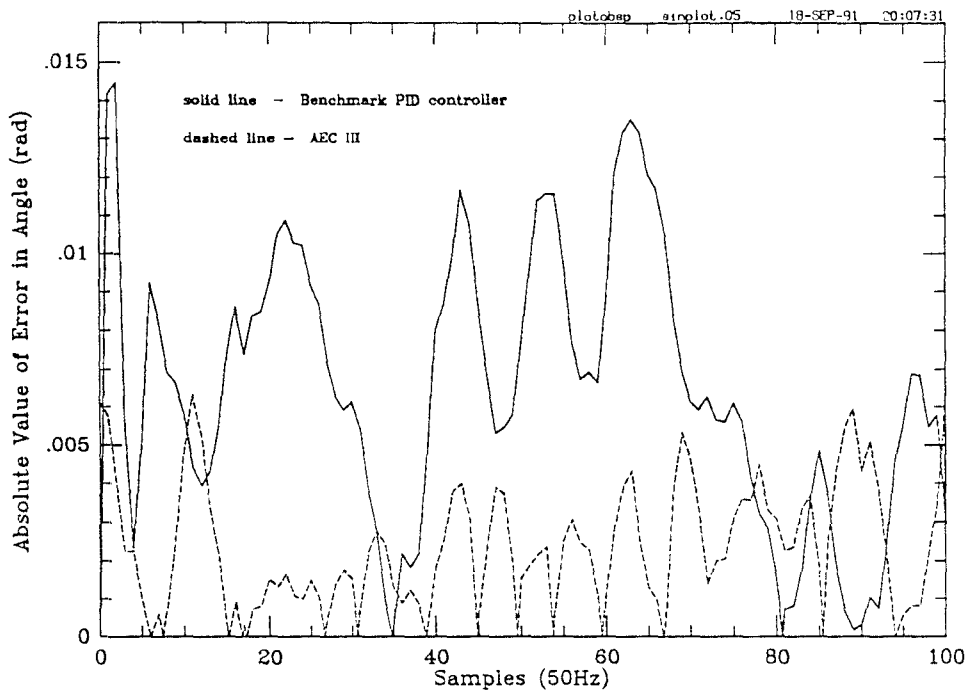

Figure 9: Position Error for AEC III Compared to Benchmark PID Controller

using Model (a) friction. The converged value of the adaptive parameter estimate $\hat{p}_2$ in these experiments indicates that the magnitude of kinetic friction is $F_k = 0.83$ lbf-in. This compares well with the expected value $F_k = 0.72$ lbf-in (average of values in positive and negative directions) as measured in the constant velocity tests performed in [7]. It seems reasonable that $\hat{p}_2$ slightly overestimates the expected value since $\hat{p}_2$ may be accounting for static friction as well as kinetic friction. The converged value of $\hat{p}_1$ was not quite as close to the value expected from previous measurements, however, the discrepancy may be due to inaccuracies in the previous measurements of motor voltage constant (note that back emf is included in the term $p_1\dot{\theta}_p$ of (8)).

Experiments using Model (b) friction showed an insignificant change in performance. This result indicates that for this set of experimental conditions, additional adaptive terms to account for friction asymmetries are not necessary. Experiments using Models (c) and (d) for friction showed only a slight improvement in performance as compared to the Model (a) experiments. Since the additional friction terms in Model (c) and

Model (d) were intended to account for Stribeck friction, this result can be attributed to the fact that Stribeck friction is probably not completely measured by the experimental system since the critical Stribeck velocity may be approximately of the same or lower order as the velocity measurement resolution.

The main disadvantage associated with AEC I was its excessively slow rate of adaptation. Although tracking performance began to improve immediately, it was not until 400 seconds into the experiment that the best results were achieved.

AEC II had the disadvantage that for the implementation that yielded the best results, the adaptive parameters tended to drift and performance deteriorated after a while. This could be avoided by resetting the parameters when they went out of a predefined range as suggested by [3] or by imposing dead-zones in the parameter update law.

AEC III, on the other hand, was very reliable and performed best of all the controllers. However, this controller is at a disadvantage in that it requires a lengthy experiment up front to determine the constants in the relationship between the friction time constant τ and the RMS velocity. Additionally, since kinetic friction T_c is held constant, AEC III is not best suited for adapting to changes in friction due to temperature or aging. This could be fixed, however, by adding an adaptive component to update T_c.

Finally, torque ripple in the motor adds a position-dependent component to the motor dynamics and could have affected how each of the controllers performed. All of the data in Table 1 applies to experiments run such that the initial position was 0.0 radians. However, it was observed that the performance of the controllers varied when different initial positions were used. To investigate this torque ripple effect, the experiment with $f = 0.5$ Hz was run again on the PID controller and AEC II and III at 15 different initial positions chosen randomly. The results of these experiments are shown in Table 2. According to these results, neither AEC II nor III performed on average as well as at an initial position of 0.0 radians. However, the greater effectiveness

Initial Position (rad)	RMS Position Error with PID Controller (rad)	% RMS Position Error Reduction from PID	
		AEC II	AEC III
-2.698	0.0086	16	23
-2.484	0.0082	26	33
-2.075	0.0091	21	23
-1.546	0.0081	30	35
-1.080	0.0079	30	39
-0.709	0.0079	28	29
-0.261	0.0072	33	36
-0.069	0.0071	32	41
0.000	0.0067	34	52
0.086	0.0068	34	46
0.689	0.0060	28	42
1.172	0.0061	15	56
1.758	0.0066	18	39
2.484	0.0076	32	37
2.720	0.0074	22	39
Average	0.0074	27	38
Std. Dev.	0.00087	6.4	8.9

Table 2: Experimental Results at Different Initial Positions ($f = 0.5$ Hz)

of AEC III relative to AEC II was observed at every initial position. From Table 2, it can be concluded that while torque ripple does affect somewhat the performance of these two adaptive controllers, it does not affect their relative effectiveness.

The effect of digital sampling rate on the performance of AEC II and III was also investigated by repeating the experiments of the experimental program with a 100 Hz sampling rate. Table 3 lists the results of these experiments. According to Table 3, the increased sampling rate did not have a dramatic effect on the performance of AEC III. However, AEC II performed significantly better with the 100 Hz sampling rate than with the 50 Hz sampling rate, particularly for experiments with $f = 0.5$ Hz and $f = 1.0$ Hz. This improved performance may be explained by the fact that overcompensation provided by AEC II for instantaneous changes in friction is not as prolonged with a 100 Hz sampling rate as it is with a 50 Hz sampling rate. Based on the results of Table 3,

Trajectory frequency f (Hz)	% RMS Position Error Reduction from PID			
	AEC II		AEC III	
	50 Hz	100 Hz	50 Hz	100 Hz
1.0	25	64	49	42
0.5	41	60	59	56
0.25	41	45	43	56
0.1	27	35	33	29

Table 3: Comparison of Tracking Experiment Results with 50 Hz and 100 Hz Sampling Rates

one can conclude that the relative effectiveness of AEC II and III is significantly affected by the digital sampling rate.

5 Conclusions

We have presented a comprehensive investigation of control strategies for friction compensation in servomechanisms performing low-velocity position tracking in the presence of velocity reversals. The major conclusions of the investigation are as follows:

- AEC I, II, and III all provide improved servomechanism position control compared to an optimized PID controller and controller with (limited frequency) dither for low-frequency sinusoidal position trajectory tracking experiments on a direct-drive dc motor. Additionally, the experimental results of this paper coupled with the results of [1, 3, 2] provide evidence for the general applicability of these adaptive and estimation-based controllers.

- The Dahl model provides a realistic and reliable model of friction, particularly during sinusoidal motion of the mechanism. Evidence for this can be found (1) in the fact that the empirically derived model of the friction time constant τ as a linear function of velocity is consistent with Dahl's original model and (2) by the relatively high effectiveness of AEC III which is based on the Dahl model. This

conclusion is noteworthy since friction is typically considered to behave according to the classical friction model.

- Mechanical considerations such as torque ripple and digital sampling rate play an important role in the performance of the adaptive and estimation-based controllers.

Further research should be pursued to understand the relationship between the classical friction model and the Dahl friction model. A determination of how to link the Dahl model of pre-sliding displacements with the classical model of sticking and sliding would provide a more complete and cohesive understanding of friction that could potentially be used to improve friction-compensating control strategies.

6 Acknowledgements

It is a pleasure to acknowledge numerous stimulating discussions on the subject of friction with Josip Lončarić. The first author is also grateful for the graduate fellowship support received from the University of Maryland Graduate School and Systems Research Center. We would also like to acknowledge critical comments from Carlos Canudas de Wit, based on an earlier draft of this paper.

References

[1] J. W. Gilbart and G. C. Winston, "Adaptive compensation for an optical tracking telescope," *Automatica*, vol. 10, pp. 125–131, 1974.

[2] C. Walrath, "Adaptive bearing friction compensation based on recent knowledge of dynamic friction," *Automatica*, vol. 20, no. 6, pp. 717–727, 1984.

[3] J. Craig, *Adaptive Control of Mechanical Manipulators.* Reading, MA: Addison-Wesley, 1988.

[4] C. Canudas, K. Astrom, and K. Braun, "Adaptive friction compensation in dc motor drives," in *Proceedings of the 1986 International Conference on Robotics and Automation*, (San Francisco, CA), pp. 1556–1561, IEEE, April 1986.

[5] B. Armstrong-Hélouvry, *Control of Machines with Friction.* Boston: Kluwer Academic Publishers, 1991.

[6] E. Rabinowicz, *Friction and Wear of Materials.* John Wiley and Sons, 1965.

[7] L. Wang, "Control system design for a flexible arm," Master's Thesis 87-164, Systems Research Center, U. of Maryland, College Park, MD, 1987.

[8] J. Courtney-Pratt and E. Eisner, "The effect of a tangential force on the contact of metallic bodies," *Proceedings of the Royal Society*, vol. A238, pp. 529–550, 1957.

[9] P. Dahl, "Measurement of solid friction parameters of ball bearings," in *Proceedings of the 6th Annual Symposium on Incremental Motion, Control Systems and Devices*, pp. 49–60, University of Illinois, 1977.

[10] E. Rabinowicz, "The intrinsic variables affecting the stick-slip process," in *Proceedings of the Physical Society of London*, pp. 668–675, 1958. Volume 71.

[11] J. Rice and A. Ruina, "Stability of steady frictional slipping," *Journal of Applied Mechanics*, vol. 50, pp. 343–349, June 1983.

[12] D. P. Hess and A. Soom, "Friction at a lubricated line contact operating at oscillating sliding velocities," *Journal of Tribology*, vol. 112, pp. 147–152, January 1990.

[13] N. E. Ehrich, "An investigation of control strategies for friction compensation," Master's Thesis 91-4, Systems Research Center, U. of Maryland, College Park, MD, 1991.

[14] C. Canudas de Wit, "Experimental results on adaptive friction compensation in robotic manipulators: low velocities," in *Lecture Notes in Control and Information*

Sciences, 139 (V. Hayward and O. Khatib, eds.), pp. 196–214, Springer-Verlag, 1989.

[15] D. Hill and P. Moylan, "The stability of nonlinear dissipative systems," *IEEE Transactions on Automatic Control*, vol. 21, pp. 708–711, October 1976.

[16] D. Hill and P. Moylan, "Stability results for nonlinear feedback systems," *Automatica*, vol. 13, pp. 377–382, 1977.

[17] M. Fan, L. Wang, J. Koninckx, and A. Tits, "CONSOLE Users Manual," Tech. Rep. 87-212, Systems Research Center, 1987.